Morphological substrates for parallel streams of corticogeniculate feedback originating in both V1 and V2 of the macaque monkey

Farran Briggs[1], **Caitlin W. Kiley**[2], **Edward M. Callaway**[3], and **W. Martin Usrey**[2]

[1]Physiology & Neurobiology, Geisel School of Medicine at Dartmouth, Lebanon NH 03755 USA

[2]Center for Neuroscience, University of California, Davis, Davis CA 95618 USA

[3]Systems Neurobiology Laboratories, Salk Institute for Biological Sciences, La Jolla CA 92037 USA

Abstract

Corticothalamic circuits are essential for reciprocal information exchange between the thalamus and cerebral cortex. Nevertheless, the role of corticothalamic circuits in sensory processing remains a mystery. In the visual system, afferents from retina to the lateral geniculate nucleus (LGN) and from LGN to primary visual cortex (V1) are organized into functionally distinct parallel processing streams. Physiological evidence suggests corticogeniculate feedback may be organized into parallel streams; however, little is known about the diversity of corticogeniculate neurons, their local computations, or the structure-function relationship among corticogeniculate neurons. We used a virus-mediated approach to label and reconstruct the complete dendritic and local axonal arbors of identified corticogeniculate neurons in the macaque monkey. Our results reveal morphological substrates for parallel streams of corticogeniculate feedback based on distinct classes of neurons in V1 and V2. These results support the hypothesis that distinct populations of feedback neurons provide independent and unique information to the LGN.

INTRODUCTION

Knowledge of the structural diversity of neurons in the brain and how they are wired together is critical for understanding how the brain processes information. New procedures for identifying specific neuronal cell types and for mapping connections between neurons with high resolution hold great promise toward advancing our understanding of the brain. Implicit in these endeavors is the assumption that structure in the brain, of individual

neurons and neural circuits, dictates function. However, the precise structure-function relationships among neurons in identified circuits have only been worked out for a small number of circuits. Our goal was to determine the morphological properties of corticogeniculate neurons in the macaque monkey to test the hypothesis that the corticogeniculate pathway is comprised of distinct cell classes with circuit properties selective for parallel streams of visual processing.

Corticothalamic feedback circuits arising from layer 6 of primary sensory cortex are ubiquitous across mammalian species and sensory modalities, and yet the functional role of these circuits for sensory processing and perception remains a fundamental mystery in neuroscience. Corticothalamic synapses onto thalamic relay neurons far outnumber those originating from peripheral sensory receptor organs such as the retina (Ahmed et al., 1994; Erisir et al., 1997a; Erisir et al., 1997b; Guillery, 1969). However the physiological responses of individual thalamic neurons tend to mimic those of their peripheral inputs and not their cortical inputs (Jones, 2007; Sherman and Guillery, 2005). For this reason, corticothalamic circuits are thought to modulate rather than drive the activity of the sensory thalamus (Sherman and Guillery, 1998). Physiological and computational results suggest that corticothalamic feedback could serve as a filter or a gate for incoming sensory information (Briggs and Usrey, 2008). However, it is unclear whether such a filtering or gating mechanism is generalized or specific to the distinct parallel processing circuits that are a hallmark of all feedforward sensory pathways.

In the visual system of mammals, corticogeniculate (CG) neurons link primary visual cortex (V1) with the lateral geniculate nucleus (LGN) of the thalamus in the feedback direction. Across a variety of species, there is evidence for multiple CG structural and/or functional organization schemes. For example, CG neurons in cats and mice display stereotyped local arborization patterns, but CG neurons in cats target layer 4 with their local axons while CG neurons in mice make stronger functional connections with layer 5 (Katz, 1987; Kim et al., 2014). Anatomical studies of primates and tree shrews indicate CG neurons in the upper and lower tiers of layer 6 preferentially innervate specific layers of the LGN (Conley and Raczkowski, 1990; Fitzpatrick et al., 1994; Ichida and Casagrande, 2002; Ichida et al., 2014; Lund et al., 1975; Usrey and Fitzpatrick, 1996), however dendritic morphologies of CG neurons could be homogeneous (Ichida et al., 2014). Physiological recordings of CG neurons in alert primates reveal distinct CG cell types carrying information related to the magnocellular, parvocellular, or koniocellular feedforward processing streams (Briggs and Usrey, 2009, 2011). Likewise, physiological studies examining CG neurons in carnivores and rabbits also conclude that the CG feedback pathway is comprised of functionally distinct neurons (Briggs and Usrey, 2005; Grieve and Sillito, 1995; Harvey, 1978; Swadlow and Weyand, 1987; Tsumoto and Suda, 1980). Thus while anatomical evidence suggests that CG circuits may not be strictly stream-specific (e.g. some CG neurons may target multiple layers in the LGN), physiological evidence suggests that CG circuits are functionally stream-specific. In order to link structure and function in the CG circuit, it is essential that we know how many functionally and morphologically distinct CG neuron types exist in the visual cortex. This is especially important in light of the fact that previous anatomical and physiological studies may be biased toward the more abundant types of CG neurons and may have missed additional and rare CG subtypes that contribute to feedback processing.

Another important goal toward understanding the role of CG feedback in visual processing is to elucidate the local circuit computations of distinct CG neuron types in order to understand the specific information each CG neuron conveys to the LGN. A prior study utilizing photo-uncaging of glutamate to map the local inputs onto individual pyramidal neurons in layer 6, including CG neurons, revealed that layer 6 pyramidal neurons of the same morphological type received similar patterns of local inputs (Briggs and Callaway, 2001). Importantly, patterns of local input were predicted by the dendritic organization of each neuron, indicating dendritic architecture provides key information about the local circuit computations performed by individual CG neurons.

In order to generate a complete survey of CG neuron types, including rare subtypes, we employed a virus-mediated labeling method that produced Golgi-like filling of individual CG neurons to reconstruct the complete dendritic arborization patterns of CG neurons in the visual cortex of the macaque monkey, including rare neuron classes not previously described or identified as projecting to the LGN. We found striking morphological evidence for multiple streams of CG feedback originating from 5 distinct types of CG neurons in V1. Importantly, we also identified at least three morphologically distinct CG neurons in V2. These results provide strong evidence in favor of a CG feedback organizational scheme involving at least three and possibly more independent streams that carry information from the visual cortex to the LGN. Through this organization scheme, CG feedback could independently filter or gate the feedforward flow of visual information. Finally, the sublaminar organization of CG feedback from V2 to the LGN forces us to rethink the modular organization of parallel processing streams within V2 as well as the role of V2 in thalamocortical communication.

RESULTS

In order to obtain a comprehensive understanding of the structural organization of CG neurons in the macaque monkey, we injected G-deleted rabies virus expressing the gene for EGFP, specifically SAD G-EGFP (Wickersham et al., 2007) into the LGN of two animals (Figure 1A and Supplemental Figure 1A) and reconstructed EGFP-expressing cortical neurons. Because this modified virus lacks the glycoprotein necessary for cell-to-cell infection, the virus cannot infect cells transsynaptically. Instead, it behaves like a retrograde tracer with the added benefit that infected cells express EGFP in a Golgi-like fashion, thus enabling full morphological reconstruction of many neurons (Figure 1 and Supplemental Figure 1B), including rare and previously undescribed neurons. Reconstructions of virus injection sites in both animals (Supplemental Figure 1A) revealed that injections were restricted to the LGN and did not encroach into surrounding structures. Injection sites included all layers of the LGN. In both animals virus was placed in multiple locations of each LGN to allow retrograde infection of CG neurons over a wide range of eccentricity (see Supplemental Figure 1A). Labeled neurons were located in layer 6 of visual cortex (described below; see Figure 1B and Supplemental Figure 1B) as well as in a variety of non-cortical structures known to provide synaptic input to the LGN, including the reticular nucleus, which lies immediately adjacent to the LGN. In one animal, we examined the basal forebrain for labeled neurons and only found two labeled cells (Supplemental Figure 2). This served as an important control for assessing the spread of virus from the injection site,

as the basal forebrain provides synaptic input to the reticular nucleus, but not to the LGN (Guillery and Harting, 2003; Jones, 2002). Labeled CG neurons in the visual cortex often formed clusters (Supplemental Figure 1B) likely due to multiple injections that were non-uniformly distributed in the LGN. CG clusters did not show any relationships to V1 cytoarchitecture and all clusters observed included multiple CG cell types.

The majority of labeled CG neurons were located in V1, as expected (Gilbert and Kelly, 1975; Lund et al., 1975). Surprisingly, labeled CG neurons were also present in V2. While their existence was suggested (Lin and Kaas, 1977), V2 CG neurons in the primate had not been previously described, in part due to the sparser distribution of CG neurons in V2 compared to V1. In both V1 and V2, CG neurons were always located in layer 6 and were typically segregated into upper and lower tiers of layer 6 (Figure 1B). We never observed labeled neurons outside of layer 6, nor did we observe labeled neurons in the opposite hemisphere, confirming that viral injections were indeed restricted to the LGN, and did not involve the ventral LGN or the adjacent pulvinar nucleus, both of which receive input from layer 5 in the visual cortex (Conley and Friederich-Ecsy, 1993; Jones, 2002; Lund et al., 1975; Rockland, 1994).

We occasionally observed neurons in extrastriate visual areas beyond V2, but we did not systematically study these rare cases. Instead we focused our examination on CG neurons in V1 and V2. Examples of labeled V1 and V2 CG neurons are shown in Figures 1C, D, and E. We reconstructed a total of 120 V1 CG neurons and 40 V2 CG neurons (see Experimental Procedures), and we quantitatively analyzed their dendritic and local axon (when possible) arborization patterns, along with their relative positions within the cortex, in order to gain insight into their local circuit connectivity and function.

CG neurons in V1

We performed independent cluster analyses (Cauli et al., 2000; Thorndike, 1953) on our sample of V1 CG neurons in order to determine whether their morphological characteristics varied systematically and to assess whether the CG pathway is comprised of morphologically distinct classes of cells. Using five morphological metrics (cell body position in layer 6, index of basal dendrite length [BD] in layer 6A vs. 6B, apical dendrite [AD] height, percentage of AD length in layer 5, and percentage of AD length in layer 2/3), the cluster analysis separated V1 CG neurons into two major groups based on strong correlations between cell body position within layer 6 and the other four metrics listed above. Neurons in the first group (left dendrogram branch in Figure 2A; n = 82) all had cell bodies in layer 6A; neurons in the second group (right dendrogram branch in Figure 2A; n = 38) all had cell bodies in the lower tier of layer 6. The leftward branch of the dendrogram contained a unique class of spiny stellate CG neurons (purple box in Figure 2A) notably distinct from all other CG neurons based on their lack of apical dendrites (see Figure 1D for two example spiny stellate CG neurons). All of the spiny stellate CG neurons had cell bodies in layer 6A. Across all CG neurons, the majority of basal dendrites were located in the same tier of layer 6 as the cell body, and CG neurons in upper and lower tiers of layer 6 differed significantly in the percentage of BD in layer 6A vs. 6B (Figure 2B; p < 0.007). It is worth noting that these restricted patterns of basal dendrite arborization match the differential

distribution of parvocellular and magnocellular LGN axon input to layer 6, with parvocellular axons sending collateral projections to the upper tier of layer 6 and magnocellular axons sending collateral projections to the lower tier of layer 6 (Conley and Raczkowski, 1990; Fitzpatrick et al., 1994; Ichida and Casagrande, 2002; Lund et al., 1975). Additionally, CG neurons in layer 6A had significantly more apical dendritic arborization in layers 5, 4Cβ, and 2/3 (Figure 2B; p < 0.007). Analyses of the number of branch points per layer yielded similar results (data not shown).

To assess the composition of V1 CG neurons further, we performed a second round of cluster analyses on upper and lower CG neurons separately, which included additional morphological metrics. When cell body size was taken into account, non-stellate upper CG neurons were further subdivided into two types: Iβ cells matching the Iβ and IβA cell types previously identified in layer 6 of V1 (Wiser and Callaway, 1996) and large cells (Figure 2C), which had some morphological features resembling Meynert cells – a specific cell type previously identified at the border between layers 5 and 6 of monkey V1 that projects to the pulvinar, area MT, and the superior colliculus (le Gros Clark, 1942; Winfield et al., 1983). When the angle at which the principal apical dendrite left the cell body was taken into account, lower CG neurons were further subdivided into two types: IC cells matching the IC cell type identified previously (Wiser and Callaway, 1996) and a group of cells we termed "tilted" cells because of a marked tilt present in the initial segment of the principal apical dendrite (Figure 2D). Tilted neurons had oval-shaped cell bodies and apical dendrites that exited the cell body from the side (rather than the top as for most pyramidal-shaped neurons) before turning to progress upward through the cortical layers toward the pial surface (see Figure 1C, rightmost picture and Figure 3, rightmost reconstruction and Supplemental Figure 3E). One hypothesis for the unique shape of tilted neurons is they were among the first cortical neurons to be born in the developing cortex (evidenced by their position at or below the layer 6/white matter border) and as the cortex expanded, the apical dendrites became stretched in the direction of cortical expansion. Along these lines, labeled neighboring tilted neurons always had apical dendrites exiting the same side of the cell body before curving up toward the pial surface and no neighboring neurons of other types demonstrated tilted cell bodies or angled apical dendrites.

In summary, based on independent clustering, we identified five types of CG neurons in V1. Separation of the five V1 CG neuron types along two dimensions (cell body position in layer 6 and cell body area) is illustrated in Figure 2E. Within our sample of reconstructed neurons, Iβ cells were the most abundant (n=57), followed by IC cells (n=26), large cells (n=19), tilted cells (n=12), and stellate cells (n=6). Images of each cell type are shown in Figures 1C and D, and representative reconstructions are shown in Figure 3 (for additional reconstructions of all identified cell types, see Supplemental Figure 3). In the remainder of this section, we consider in greater detail the quantitative features that distinguish CG neurons of each cell type.

Across the five cell types, there were significant differences in cell body position within layer 6 (Figure 2F), cell body area (Figure 2G), and the angle at which the AD exited the cell body (Figure 2H). Specifically, the cell bodies of Iβ, large, and spiny stellate cells were positioned more superficially than the cell bodies of IC and tilted cells (p = 5.1×10-7). Large

CG neurons had significantly larger cell bodies compared to all other V1 CG neurons (p = 2.2×10-9). Tilted CG neurons were unique in two key features. First, the positions of all tilted cells within the same narrow band of cortex at the layer 6/white matter border were highly consistent as evidenced by the lowest variance in cell body position within layer 6 among all of the cell types (Figure 2E; tilted cell body positions were also significantly deeper in layer 6 relative to IC cell body positions, p = 3.6×10^{-4}). Second, the angle at which the principal apical dendrite exited the cell body relative to a straight line drawn between the center of the cell body and the pial surface were significantly greater in tilted neurons compared to all other V1 CG neurons (p = 4.6×10^{-8}). Tilted neurons were distributed throughout the cortex (e.g., not restricted to regions of cortical curvature – see Supplemental Figure 1B, neuron marked by leftmost arrow) and non-tilted CG neurons neighboring tilted neurons did not demonstrated angled apical dendrites or cell bodies.

In order to gain insight into the local circuitry involving V1 CG neurons of each cell type, we quantified the percentage of dendrite within the different cortical layers. Consistent with their relative cell body position in layer 6, upper CG neuron types (Iβ, large, spiny stellate) differed significantly from lower CG neuron types (IC, tilted) in the amount of basal dendrite in layer 6A vs. 6B (quantified by an index of BD length in layer 6A vs. 6B, see Experimental Procedures; p = 4×10^{-18}; Figure 4A). Interestingly, large and Iβ CG neurons differed significantly in their indices of BD in layer 6A vs. 6B as large neurons had more basal dendrites in layer 6B even though their cell bodies were positioned in layer 6A (Figure 4A, see also Figures 1D and 3 for examples). Iβ and large CG neurons had significantly higher percentages of AD in layer 5 compared to spiny stellate neurons (which, by definition, lacked apical dendrites), IC, and tilted CG neurons (p = 1×10^{-10}; Figure 4B). Iβ CG neurons also had significantly more AD within layer 2/3 compared to IC and tilted CG neurons (p = 0.007; Figure 4C). Although most V1 CG neurons showed no preference for dendritic arborization in the different sublaminar divisions of layer 4C, Iβ neurons preferentially targeted layer 4Cβ with their apical dendrites (p = 3.4×10^{-4}; Figure 4D).

For a subset of V1 CG neurons, we were able to reconstruct local axonal arbors within V1. Our sample of V1 CG neurons with axons included 13 Iβ cells, 3 large cells, 5 IC cells, and 5 tilted cells. We first quantified the average percentage of axon per layer for upper and lower CG neurons (Figure 5A). Upper CG neurons had significantly more axonal arborization in layer 4Cβ, while lower CG neurons had significantly more axonal arborization in layer 6B (p < 0.007). Percentages of axons in layer 6A vs. 6B were consistent with cell body positions within the sublaminae (Figure 5B), and indices of axon in layer 6A vs. 6B differed significantly between Iβ and both IC and tilted CG cell types (p = 0.0004). In a similar pattern to that observed for apical dendrites, only Iβ CG neurons displayed significantly greater axonal arborization in layer 4Cβ over layer 4Cα (p = 3.3×10^{-5}; Figure 5C).

CG neurons in V2

As with our sample of V1 CG neurons, we conducted an independent cluster analysis to determine whether morphological characteristics varied systematically across V2 CG neurons and to assess whether the CG pathway originating in V2 is comprised of

morphologically distinct classes of cells. Cluster analysis of 40 reconstructed V2 CG neurons based on the same five morphological metrics applied to V1 neurons revealed two groups of V2 CG neurons based again on strong correlations between the position of cell bodies in layer 6 and the other four morphological metrics (Figure 6A). The right branch of the cluster dendrogram contained 17 V2 CG neurons all with cell bodies positioned in layer 6A, while the left branch of the dendrogram contained 23 V2 CG neurons with cell bodies positioned in layer 6B. Further, we were able to reconstruct the local axon arbors of 8 upper CG neurons and 12 lower CG neurons in V2. Three example V2 CG neurons are illustrated in Figure 1E, including one upper CG neuron (left) and two lower CG neurons (middle, right). Figure 6B shows representative reconstructions of one upper (left) and two lower (middle, right) CG neurons in V2 (for additional V2 reconstructions, see Supplemental Figure 3F). Due to the smaller sample size, we did not attempt to subdivide upper or lower V2 CG neurons further; however, it is possible that upper and lower CG neurons in V2 could each consist of multiple distinct cell types similar to V1 CG neurons. While most lower CG neurons in V2 resembled V1 CG neurons of the IC cell type, five lower V2 CG neurons resembled V1 tilted CG neurons (examples in Figures 1E and 6B, rightmost in each) and three of these five were located in the leftmost sub-branch of the lower layer 6 CG neuron cluster (blue box in Figure 6A). Thus the cluster analysis suggests a trend whereby lower CG neurons in V2 could be separated into two distinct cell classes (resembling V1 CG neurons of the IC and tilted cell types) given a larger sample size.

Similar to V1 CG neurons, V2 CG neurons in upper and lower tiers of layer 6 differed significantly in their basal and apical dendritic arborization patterns (Figure 6C). The majority of basal dendrites were again located in the same tier of layer 6 as the cell body, and upper and lower V2 CGs differed significantly in the percentage of BD in layer 6A vs. 6B (Figure 6C; $p < 0.003$). Upper V2 CGs also had significantly more apical dendritic arborization in layer 5 ($p < 0.003$), however upper and lower V2 CGs did not differ in their apical dendritic arborization patterns in layers 4 or 2/3 (Figure 6C). Cell body position and area both differed significantly between upper and lower CG neurons in V2 ($p = 1.5 \times 10^{-7}$ and $p = 0.046$, respectively; Figure 6D). Consistent with their different cell body positions in layer 6, upper and lower CG neurons also differed significantly in indices of BD length in layer 6A vs. 6B ($p = 6.4 \times 10^{-8}$; Figure 6E). Upper CG neurons also had significantly more AD length in layer 5 compared to lower CG neurons in V2 ($p = 0.002$; Figure 6F), similar to CG neurons in V1. Interestingly, lower CG neurons in V2 had significantly more axonal arborization in layer 2/3 compared to upper CG neurons in V2 ($p = 0.03$; Figure 6G).

In summary, independent clustering identified at least two distinct types of CG neurons in V2. CG neurons in V2 shared a number of morphological features with V1 CG neurons, including relationships between cell body position in layer 6A or 6B and arborization patterns in the overlying cortical layers. Interestingly, the three main types of CG neurons in V1 (Iβ, IC, and tilted cells) mirrored the three most frequently observed morphological types in V2 (upper V2 CG neurons resembled Iβ cells while lower V2 CG neurons resembled IC or tilted cells) suggesting that morphological substrates for parallel streams could be a conserved property of CG circuits.

DISCUSSION

The functional role of corticothalamic feedback in sensory perception, and the specific role of CG circuits in vision, have remained fundamental and unresolved questions in systems neuroscience. Anatomical and physiological evidence from a variety of mammalian species support different organizational schemes for CG circuits, including evidence that CG circuits are comprised of multiple distinct cell types suggestive of stream-specific organization (Briggs and Callaway, 2001; Briggs and Usrey, 2007, 2009; Conley and Raczkowski, 1990; Fitzpatrick et al., 1994; Harvey, 1978; Ichida and Casagrande, 2002; Lund et al., 1975; Swadlow and Weyand, 1987; Tsumoto and Suda, 1980; Usrey and Fitzpatrick, 1996; Wiser and Callaway, 1996) and evidence that CG circuits are comprised of homogeneous cell types suggestive of feedback to overlapping LGN layers (Ichida et al., 2014; Katz, 1987). Due to sparse CG neuron distributions (in the macaque monkey, only ~14% of layer 6 neurons are CG neurons (Fitzpatrick et al., 1994)) and potential biases of traditional anatomical and physiological measurements toward more common CG cell types, the precise structural organization of CG feedback has been difficult to establish. In spite of these challenges, morphometric analyses of large samples of CG neurons are essential for understanding the structural organization of CG circuits and their functional contributions to local circuit and LGN computations. We have overcome potential biases of previous methodologies by utilizing a novel anatomical technique that harnesses the power of viruses to drive expression of fluorescent proteins and generate Golgi-like fills of CG neurons selectively. With this technique, we surveyed a broad distribution of CG cell types in the macaque monkey, including cell types not previously described or identified as projecting to the LGN. We performed independent cluster analyses of 160 CG neurons using a variety of morphological metrics ascertained from single-neuron reconstructions, and we identified multiple distinct CG cell types in both V1 and V2 (Figure 7). These cell types, each with distinct morphology indicative of their connectivity within the cortical architecture, provide strong support for the view that the CG pathway consists of multiple streams, each conveying distinct information to specific targets in the LGN.

Previous anatomical studies identified a relationship between CG neurons located in the upper and lower tiers of layer 6 and the parvocellular and magnocellular layers of the primate LGN, respectively (Conley and Raczkowski, 1990; Fitzpatrick et al., 1994; Ichida and Casagrande, 2002; Lund et al., 1975). In agreement with these studies, our morphometric analysis of CG neurons in V1 likewise distinguished two main groups of CG neurons that segregate into upper and lower tiers of layer 6. Within these two main groups were additional, morphologically distinct cell types with dendritic and axonal arborization patterns indicative of their involvement in circuit-specific processing of visual signals. In general, CG neurons in upper layer 6 made more local connections to the overlying layers in V1, while CG neurons in layer 6B were more strongly interconnected to neighboring neurons within layer 6B. Upon closer examination, we identified three types of CG neurons in upper layer 6. One group of upper layer 6 neurons, the Iβ CG neurons, displayed a strong relationship with the parvocellular-recipient layer 4Cβ and also layer 2/3, as evidenced by selective dendritic and axonal arborization within these layers. These results are consistent with photostimulation experiments demonstrating functional inputs onto Iβ neurons

originating from layers 4C and 2/3 (Briggs and Callaway, 2001) and further support the notion that CG neurons in upper layer 6 project to the parvocellular layers of the LGN (Fitzpatrick et al., 1994). Although our study was focused on the morphometric properties of CG neurons and did not measure visual physiology, the local circuit connections of Iβ CG neurons likely endow these neurons with simple cell receptive fields and parvocellular-like physiological response properties, consistent with physiological recordings from identified CG neurons (subtype unknown) in upper layer 6 (Briggs and Usrey, 2009). In contrast to the Iβ CG neurons, the other two groups of upper layer 6 CG neurons—the large CG neurons and the spiny stellate CG neurons—sampled more local information within layer 6 and demonstrated no bias in either dendritic or axonal projections to the subdivisions of layer 4C. Given that large and spiny stellate CG neurons may not have as strong a relationship to the parvocellular-recipient layer in V1 compared to Iβ CG neurons, it is possible that these two CG cell types make up additional feedback processing channels. Prior anatomical studies have found evidence for both stream-specific and stream-mixed CG feedback in primates (Fitzpatrick et al., 1994; Ichida and Casagrande, 2002; Ichida et al., 2014). It is therefore possible that Iβ CG neurons provide parvocellular-stream-specific feedback while large and spiny stellate neurons provide feedback to specific combinations of parvocellular and koniocellular LGN neurons.

Our analysis identified two groups of CG neurons with cell bodies in layer 6B, the IC neurons and the tilted neurons. Although the dendritic arbors of IC neurons did not show a preference for layer 4Cα (the cortical target of magnocellular LGN axons), functional local inputs to these neurons have a magnocellular bias, originating preferentially from layers 4B and 5 (Briggs and Callaway, 2001). Past anatomical work in the macaque has shown a strong connection between neurons in the lower tier of layer 6 and the magnocellular layers of the LGN (Fitzpatrick et al., 1994). Given the local circuitry associated with the IC CG neurons, it seems likely that these neurons are the source of input to the magnocellular layers. These neurons are also likely to be complex cells with magnocellular-like physiological responses, consistent with the physiological properties associated with a subset of lower layer 6 CG neurons (Briggs and Usrey, 2009). CG neurons in the final group, the tilted neurons, share a characteristic morphology that resembles "displaced" and "tangential" pyramidal neurons described previously in rat and cat visual cortex (Miller, 1988; Tombol, 1984). Anatomical results from the macaque and other species also support a relationship between lower layer 6 CG neurons and the koniocellular (or konio-equivalent) layers of the LGN (Bourassa and Deschenes, 1995; Fitzpatrick et al., 1994; Ichida and Casagrande, 2002; Ichida et al., 2014; Usrey and Fitzpatrick, 1996). Along these lines, Briggs and Usrey (Briggs and Usrey, 2009) observed CG neurons located deep in layer 6 of the macaque monkey that displayed koniocellular-like response properties. Thus, based on their position in the deepest zone at the layer 6/white matter border, tilted CG neurons are candidate koniocellular-projecting CG neurons. An alternative interpretation of deep layer CG neurons is that both IC and tilted CG cell types provide unique and stream-mixed feedback to specific magnocellular and koniocellular LGN neurons. The fact that neither IC nor tilted CG neurons preferentially connect with layer 4Cα suggests that there may not be a purely magnocellular-specific feedback projection (but see above description of local functional inputs to IC neurons). If IC and tilted CG neurons are the fast-conducting complex and slow-conducting complex CG

neurons identified physiologically, then their structure-function relationships suggest they are separate feedback channels, regardless of their projection targets within the LGN.

A particularly surprising finding of this study was the identification of morphologically distinct groups of CG neurons in V2. Lin and Kaas (Lin and Kaas, 1977) described sparse connectivity between V2 and LGN in the primate based on proline injections in cortex and labeling in LGN, however to the best of our knowledge, no prior study has described the morphology of V2 CG neurons. Our results demonstrate that V2 CG neurons share many features in common with V1 CG neurons, including a robust relationship between cell body position in layer 6 and the distribution of basal dendrites within the layer. Likewise, V2 CG neurons in layer 6A display stronger patterns of connectivity with cortical layer 5 than CG neurons in layer 6B. However, in contrast to V1 CG neurons, V2 CG neurons in layer 6B are more strongly coupled to layer 2/3 compared to V2 CG neurons in layer 6A. Based on homology with V1, it is tempting to predict that upper CG neurons in V2 project to the parvocellular layers in the LGN while lower CG neurons project to the magnocellular and possibly koniocellular layers. However, given the limited information available about local circuitry within V2 and a lack of information about the visual physiology of V2 CG neurons, one cannot rule out the possibility that V2 CG neurons follow a different set of rules regarding their patterns of projection within the LGN. Nevertheless, the presence of CG neurons in V2 with morphological phenotypes that not only indicate differential connectivity within the architecture of V2 but also display a sublaminar organization within layer 6 suggests there exists a laminar/sublaminar organization of parallel processing that operates in tandem with the well-recognized columnar organization—the "thick," "thin," and "pale" stripes—of V2 (Livingstone and Hubel, 1984; Roe and Ts'O, 1999; Sincich and Horton, 2005).

Results from numerous theoretical, physiological, and anatomical studies have led to predictions about the functional role of CG circuits in vision (Briggs and Usrey, 2008, 2011). These include suggestions that CG feedback serves as a filter or gate for salient visual signals arriving from the environment and/or CG feedback carries cognitive signals to facilitate the effects of attention on visual processing. Results from the current study hone these hypotheses and also support an expanded view of the functional role of CG neurons. First, our morphological results provide clear evidence for distinct classes of CG neurons that provide the substrate for multiple parallel streams of CG feedback to the LGN. Therefore, any filtering/gating mechanisms or conduits of cognitive signals are operating through separate CG circuits. With this view, a number of testable predictions follow, including the notion that filtering and/or attentional modulation may occur at different time scales depending on the CG circuit involved given that CG neurons projecting to magno-, parvo-, and koniocellular layers in the LGN have distinct visual response latencies and axon conduction velocities (Briggs and Usrey, 2007, 2009). Second, it is important to consider the target specificity of both the extrinsic (LGN-projecting) and intrinsic axons from CG neurons when considering the influence of CG neurons on the processing of visual signals. Because CG neurons innervate both the LGN and the targets of LGN afferent projections, CG neurons are uniquely positioned to influence visual signals delivered to cortex. Additionally, CG neurons in both upper and lower tiers of V1 and V2 project local axons throughout the cortical depth including the superficial layers and layer 5, both of which

contain cortico-cortical projecting neurons. CG neurons are therefore well suited to influence not only visual signals relayed through the thalamus but also visual signals transmitted to higher cortical areas.

Overall, the structural organization of CG feedback, as evidenced by the existence of at least five distinct CG cell types in V1 and at least three distinct CG cell types in V2, predicts that there are multiple distinct channels of CG feedback. It is likely that in addition to stream-specific feedback to the magnocellular and parvocellular LGN layers, there are additional feedback channels, possibly targeting stream-mixed populations of LGN neurons. The fact that CG feedback originates in both V1 and V2 indicates that cortical control of visual processing in the LGN is a multi-step process. Feedback from the two cortical areas could serve similar functions at different spatial scales, e.g., feedback from V2 could synchronize the activity of larger populations of LGN neurons compared to feedback from V1. Alternatively, feedback from each area could convey top-down influences that modulate separate LGN populations according to the feature preferences of the activated CG cell types. Future studies employing cell-type specific recordings and/or manipulations will be required to unravel the functional role of V2 CG neurons, including their visual physiology and specific targets within the LGN.

EXPERIMENTAL PROCEDURES

Two adult male macaque monkeys (*Macacca mulatta*) were used in this study. All procedures involving animals were approved by the Institutional Animal Care and Use Committees at UC Davis and the Salk Institute and conformed to the guidelines set forth by the USDA and NIH. In order to label corticogeniculate (CG) neurons in the visual cortex selectively, modified rabies virus carrying the gene encoding EGFP (SAD G-EGFP, based on the SAD-B19 strain (Wickersham et al., 2007)) was injected into the lateral geniculate nucleus (LGN) of the thalamus. Because SAD G-EGFP lacks the gene encoding an essential glycoprotein (G-gene), the virus cannot move transsynaptically and instead acts like a retrograde tracer. It is taken up by axon terminals at the injection site (in this case the LGN) and moves in a retrograde direction to the cell body where it replicates and expresses EGFP in infected neurons. The main advantage of using SAD G-EGFP over conventional retrograde tracers is that infected neurons express EGFP throughout their dendritic and axonal arbors, allowing for more complete reconstruction of neuronal morphology. Unlike other types of viruses, rabies virus is extremely efficient as a retrograde tracer, as demonstrated previously (Callaway, 2009; Osakada et al., 2011; Wickersham et al., 2007).

Virus injection

All surgical procedures were conducted in a sterile environment using aseptic techniques. Animals were initially anesthetized with ketamine and then maintained under full surgical anesthesia with isoflurane (1-3% inhaled in oxygen or a 2:1 mixture of oxygen and nitrous oxide). Animals were placed in a stereotaxic frame and wrapped in a thermostatically controlled heating blanket. Throughout surgical procedures, animals were continuously monitored for heart rate, respiration rate, expired CO_2, SPO_2, and temperature. A midline scalp incision was made and the muscles retracted. A small craniotomy was made according

to stereotaxic coordinates for the LGN in one hemisphere. A platinum/iridium or tungsten recording electrode (FHC, Bowdoin, ME) was lowered through the craniotomy into the brain and neuronal responses to light flashes in the eyes were used to determine the location, depth, and thickness of the LGN. The recording electrode was removed and an injection pipette (glass pipette or Hamilton syringe) was placed in the same stereotaxic location identified from physiological recordings and lowered to the appropriate depth. Injections were made at multiple depths throughout the LGN using a picospritzer or by pressure applied to the Hamilton syringe. A total volume of 30 microliters of virus was injected into a single LGN in Monkey 1 over 6 separate injection sites (in LGN layers 1-6) and a total volume of 5 microliters of virus was injected into a single LGN in Monkey 2 over 4 separate injection sites (in LGN layers 1, 2, 4, and 5). Injected virus did not fill the entire LGN, but covered similar proportions of LGN in each animal, spanning all layers of the LGN and multiple eccentricities (Supplemental Figure 1A). The injection pipette was removed, the bone piece was glued in place with Vetbond in one animal and gel foam and bone wax was placed over the craniotomy in the other, and the muscles and skin were sutured together. Animals recovered for 7 days and then were euthanized and perfused transcardially with 4% paraformaldehyde, followed by 4% paraformaldehyde with 10% sucrose, and then 20% sucrose. The brains were removed and placed in 20-30% sucrose with 4% paraformaldehyde in 0.1M phosphate buffer. For Monkey 1, a tissue block containing the LGN and visual cortex from the injected hemisphere was flash frozen and maintained at −80 degrees for 8 months prior to sectioning and histology. For Monkey 2, sectioning and histology were performed 2 days after the perfusion. Retinas for both monkeys were also preserved and observations of EGFP-labeled retinal ganglion cells in both animals confirmed successful virus injection and infection.

Staining

Tissue from both monkeys was sectioned coronally at a thickness of 50 microns per section. All sections were first stained for cytochrome oxidase activity in order to visualize cortical layers and subcortical nuclei. All sections were then labeled with a primary antibody against GFP (rabbit anti-GFP, Molecular Probes/Life Technologies, Grand Island, NY) and a secondary antibody tagged with biotin (biotinylated goat anti-rabbit, Vector Laboratories, Burlingame, CA) in order to facilitate avidin/biotin and DAB/peroxidase reactivity such that all labeled neurons were permanently stained. Sections were then mounted on glass slides, defatted, and cover slipped. We did not see clear and consistent cytochrome oxidase blobs in layer 2/3 of V1 throughout or samples, so we did not analyze relationships between labeled CG neurons and columns as defined by positions of blobs/interblobs.

Neuronal reconstructions and data analysis

All reconstructions were made using a Neuroludica system (MicroBrightField; Williston, VT) with a Lucivid microdisplay attached to a Nikon E800 microscope. Injection sites within the LGN of Monkey 1 and Monkey 2 were reconstructed by following the contours of the largest extent of virus label in each section through the full extent of the injection. Contours plots indicating the LGN, reticular nucleus, ventral LGN, and neighboring thalamic structures were generated and markers were placed to indicate the centers for each of the 6 (Monkey 1) and 4 (Monkey 2) separate injections (Supplemental Figure 1A).

A total of 160 CG neurons (120 V1 CG neurons and 40 V2 CG neurons) were reconstructed from both animals. From Monkey 1, 89 V1 and 20 V2 CG neurons were reconstructed and from Monkey 2, 31 V1 and 20 V2 CG neurons were reconstructed. Labeled CG neurons were selected for reconstruction when they were reasonably isolated from neighboring labeled neurons such that all neuronal processes could be unambiguously identified as a part of the same neuron. Care was taken to reconstruct neurons from different regions of V1 (e.g., from different eccentricities) in order to sample CG neurons from throughout V1. Neuronal reconstructions included cell body, basal dendrites (BD), apical dendrite (AD), and axon (when possible). Branch points were designated by nodes in the Neuroludica program. Spines were not reconstructed, but were observed throughout the dendrites of all CG neurons. Markers were placed to define the cell body position within layer 6, the cortical thickness at the position of the cell body, the highest point (toward the pial surface) along the apical dendritic arbor, and the angle at which the AD exited the cell body. Laminar boundaries were also reconstructed based on the cytochrome staining in the section containing the cell body. Layer 6 was divided into two sublayers with equal thickness, termed 6A and 6B. Reconstructions included processes extending across multiple sections (typically 3-5 sections). The following data were extracted from Neurolucida for detailed analysis: lengths of BD, AD, and axon per layer; number of nodes per layer; cell body area and position; angle of AD exiting the cell body; laminar zones and cortical thickness. All measures of BD, AD, and axon length, and nodes per layer were normalized by the total length of BD, AD, axon, and nodes per reconstruction, respectively. Laminar positions (of cell body, height of AD) were normalized by laminar and cortical thickness. An index of the percentage of BD in layer 6A vs. 6B was calculated for each reconstruction based on the following equation: (percentage of BD in 6A – percentage of BD in 6B) / (percentage of BD in 6A + percentage of BD in 6B). Similarly, an index of axon in layer 6A vs. 6B was calculated for reconstructions that included axons using the equation: (percentage of axon in 6A – percentage of axon in 6B) / (percentage of axon in 6A + percentage of axon in 6B).

Separate cluster analyses were performed in order to classify V1 and V2 CG neurons into distinct cell types based on various morphological metrics. Independent clustering algorithms form the basis for cluster analyses (Cauli et al., 2000; Thorndike, 1953) in which each sample is plotted in an n-dimensional space (n defined by the number of parameters or metrics describing each sample) and the distance between samples is calculated using a specified measurement (e.g., Euclidean distance, squared distance). All parameters defining each sample are equally weighted. For all cluster analyses used in this study, object distances were calculated based on Euclidean distance and linkages were based on inner squared distance (Ward's method) or weighted center of mass distance because these are the most basic (standard) measurements used in cluster analyses and because both measurements yielded similar results in each cluster analysis. Because each of the metrics designated below were independent and equally weighted, removing one metric from the cluster analysis did not typically result in dramatic redistribution of clusters. Likewise, additional metrics beyond those selected (the most informative metrics, described below) did not change the clusters. Finally, metrics that were only available for subsets of CG neurons in our sample (axon metrics) were not included in any cluster analyses.

For initial clustering of both V1 and V2 CG neurons, the following 5 parameters were used: cell body position in layer 6, index of BD length in layer 6A vs. 6B, AD height, percentage of AD length in layer 5, and percentage of AD length in layer 2/3. Cluster analyses of V1 and V2 CG neurons both identified two distinct classes of neurons that were distinguished based on the location of their cell bodies in layer 6A or 6B. For V1 CG neurons, a second round of cluster analyses was performed to further classify upper and lower CG neurons based on additional morphological metrics. Spiny stellate CG neurons in V1 were excluded from the upper V1 CG cluster analysis because they were identified as a distinct subclass in the initial V1 CG cluster analysis (see Figure 2A). The morphology metrics used for the second round of cluster analyses were cell body area, AD height, and index of BD length in layer 6A vs. 6B (for upper V1 CG neurons); and cell body position, percentage of AD length in layer 5, and AD angle (for lower V1 CG neurons). Based entirely on the results of the cluster analyses, V1 CG neurons were categorized into 5 classes (IB, large, spiny stellate, IC, tilted), many of which displayed homology with previously defined cell types in layer 6. V2 CG neurons formed two clusters (upper and lower V2 CG neurons). Separate from the cluster analysis, statistical comparisons of BD, AD, axon lengths, apical dendrite angle, cell body area and position were made across the defined cell classes. A non-parametric multiple comparisons test (Kruskal Wallis one-way analysis of variance) was used to determine significant differences in various morphological metrics across cell classes. Two sample comparisons were made with the Wilcoxon rank-sum test. Averages of normalized BD, AD, and axon length per layer were calculated for upper and lower V1 CG neurons. Wilcoxon rank-sum tests with Bonferroni-corrected p values were used to test significant differences in laminar arborization patterns for upper versus lower V1 CG neurons.

Supplementary Material

Refer to Web version on PubMed Central for supplementary material.

ACKNOWLEDGEMENTS

REFERENCES

Ahmed B, Anderson JC, Douglas RJ, Martin KAC, Nelson JC. Polyneuronal innervation of spiny stellate neurons in cat visual cortex. J Comparative Neurology. 1994; 341:39–49.

Bourassa J, Deschenes M. Corticothalamic projections from the primary visual cortex in rats: a single fiber study using biocytin as an anterograde tracer. Neuroscience. 1995; 66:253–263. [PubMed: 7477870]

Briggs F, Callaway EM. Layer-specific input to distinct cell types in layer 6 of monkey primary visual cortex. J Neurosci. 2001; 21:3600–3608. [PubMed: 11331389]

Briggs F, Usrey WM. Temporal properties of feedforward and feedback pathways between thalamus and visual cortex in the ferret. Thalamus and Related Systems. 2005; 3:133–139. [PubMed: 18176624]

Briggs F, Usrey WM. A fast, reciprocal pathway between the lateral geniculate nucleus and visual cortex in the macaque monkey. J Neurosci. 2007; 27:5431–5436. [PubMed: 17507565]

Briggs F, Usrey WM. Emerging views of corticothalamic function. Current Opinion in Neurobiology. 2008; 18:403–407. [PubMed: 18805486]

Briggs F, Usrey WM. Parallel processing in the corticogeniculate pathway of the macaque monkey. Neuron. 2009; 62:135–146. [PubMed: 19376073]

Briggs F, Usrey WM. Corticogeniculate feedback and parallel processing in the primate visual system. J Physiology. 2011; 589:33–40.

Callaway EM. Transneuronal circuit tracing with neurotropic viruses. Current Opinion in Neurobiology. 2009; 18:1–7.

Cauli B, Porter JT, Tsuzuki K, Lambolez B, Rossier J, Quenet B, Audinat E. Classification of fusiform neocortical interneurons based on unsupervised clustering. PNAS. 2000; 97:6144–6149. [PubMed: 10823957]

Conley M, Friederich-Ecsy B. Functional organization of the ventral lateral geniculate complex of the tree shrew (Tupaia belangeri): II. Connections with the cortex, thalamus, and brainstem. Journal of Comparative Neurology. 1993; 328:21–42. [PubMed: 7679121]

Conley M, Raczkowski D. Sublaminar organization within layer 6 of the striate cortex in galago. J Comp Neurol. 1990; 302:425–436. [PubMed: 1705271]

Erisir A, Van Horn SC, Bickford ME, Sherman SM. Immunocytochemistry and distribution of parabrachial terminals in the lateral geniculate nucleus of the cat: a comparison with corticogeniculate terminals. J Comp Neurol. 1997a; 377:535–549. [PubMed: 9007191]

Erisir A, Van Horn SC, Sherman SM. Relative numbers of cortical and brainstem inputs to the lateral geniculate nucleus. PNAS. 1997b; 94:1517–1520. [PubMed: 9037085]

Fitzpatrick D, Usrey WM, Schofield BR, Einstein G. The sublaminar organization of corticogeniculate neurons in layer 6 of macaque striate cortex. Visual Neurosci. 1994; 11:307–315.

Gilbert CD, Kelly JP. The projections of cells in different layers of the cat's visual cortex. J Comp Neurol. 1975; 163:81–106. [PubMed: 1159112]

Grieve KL, Sillito AM. Differential properties of cells in the feline primary visual cortex providing the corticofugal feedback to the lateral geniculate nucleus and visual claustrum. J Neurosci. 1995; 15:4868–4874. [PubMed: 7623117]

Guillery RW. A quantitative study of synaptic interconnections in the dorsal lateral geniculate nucleus of the cat. Z Zellfrosch. 1969; 96:39–48.

Guillery RW, Harting JK. Structure and connections of the thalamic reticular nucleus: advancing views over half a century. J Comp Neurol. 2003; 463:360–371. [PubMed: 12836172]

Harvey AR. Characteristics of corticothalamic neurons in area 17 of the cat. Neuroscience Letters. 1978; 7:177–181. [PubMed: 19605109]

Ichida JM, Casagrande VA. Organization of the feedback pathway from striate cortex (V1) to the lateral geniculate nucleus (LGN) in the owl monkey (aotus trivirgatus). J Comp Neurol. 2002; 454:272–283. [PubMed: 12442318]

Ichida JM, Mavity-Hudson JA, Casagrande VA. Distinct patterns of corticogeniculate feedback to different layers of the lateral geniculate nucleus. Eye and Brain. 2014; 6:57–73. [PubMed: 25892906]

Jones EG. Thalamic organization and function after Cajal. Progress in Brain Research. 2002; 136:333–357. [PubMed: 12143393]

Jones EG. Calcium channels in higher-level brain function. Proceedings of the National Academy of Science. 2007; 104:17903–17904.

Katz LC. Local circuitry of identified projection neurons in cat visual cortex brain slices. J Neurosci. 1987; 7:1223–1249. [PubMed: 3553446]

Kim J, Matney CJ, Blankenship A, Hestrin S, Brown SP. Layer 6 corticothalamic neurons activate a cortical output layer, layer 5a. J Neuroscience. 2014; 34:9656–9664. [PubMed: 25031405]

le Gros Clark WE. The cells of Meynert in the visual cortex of the monkey. Journal of Anatomy. 1942; 76:369–376. [PubMed: 17104906]

Lin CS, Kaas JH. Projections from cortical visual areas 17, 18, and MT onto the dorsal lateral geniculate nucleus in owl monkeys. J Comparative Neurology. 1977; 173:457–474.

Livingstone MS, Hubel DH. Anatomy and physiology of a color system in the primate visual cortex. J Neurosci. 1984; 4:309–356. [PubMed: 6198495]

Lund JS, Lund RD, Hendrickson AE, Bunt AH, Fuchs AF. The origin of efferent pathways from the primary visual cortex, area 17, of the macaque monkey as shown by retrograde transport of horseradish peroxidase. J Comp Neurol. 1975; 164:287–303. [PubMed: 810501]

Miller MW. Maturation of rat visual cortex: IV. The generation, migration, morphogenesis, and connectivity of atyipcally oriented pyramidal neurons. J Comparative Neurology. 1988; 274:387–405.

Osakada F, Mori T, Cetin A, Marshel JH, Virgen B, Callaway EM. New rabies virus varients for monitoring and manipulating activity and gene expression in defined neural circuits. Neuron. 2011; 71:617–631. [PubMed: 21867879]

Rockland KS. Further evidence for two types of corticopulvinar neurons. NeuroReports. 1994; 5:1865–1868.

Roe AW, Ts'O DY. Specificity of color connectivity between primate V1 and V2. J Neurophys. 1999; 82:2719–2730.

Sherman SM, Guillery RW. On the actions that one nerve cell can have on another: distinguishing "drivers" from "modulators". PNAS. 1998; 95:7121–7126. [PubMed: 9618549]

Sherman, SM.; Guillery, RW. Exploring the thalamus and its role in cortical function. 2nd. MIT Press; Boston: 2005.

Sincich LC, Horton JC. The circuitry of V1 and V2: intergration of color, form, and motion. Annu Rev Neurosci. 2005; 28:303–326. [PubMed: 16022598]

Swadlow HA, Weyand TG. Corticogeniculate neurons, corticotectal neurons, and suspected interneurons in visual cortex of awake rabbits: receptive-field properties, axonal properties, and effects of EEG arousal. J Neurophys. 1987; 57:977–1001.

Thorndike RL. Who belongs in the family? Psychometrika. 1953; 18:267–276.

Tombol, T. Layer VI cells. In: Peters, A.; Jones, EG., editors. Cerebral Cortex. Plenum Press; New York: 1984. p. 479-519.

Tsumoto T, Suda K. Three groups of cortico-geniculate neurons and their distribution in binocular and monocular segments of cat striate cortex. J Comp Neurol. 1980; 193:223–236. [PubMed: 7430428]

Usrey WM, Fitzpatrick D. Specificity in the axonal connections of layer 6 neurons in tree shrew striate cortex: evidence for distinct granular and supragranular systems. J Neurosci. 1996; 16:1203–1218. [PubMed: 8558249]

Wickersham IR, Finke S, Conzelmann KK, Callaway EM. Retrograde neuronal tracing with a deletion-mutant rabies virus. Nature Methods. 2007; 4:47–49. [PubMed: 17179932]

Winfield DA, Neal JW, Powell TP. The basal dendrites of Meynert cells in the striate cortex of the monkey. Proc R Soc Lond Biol Sci. 1983; 217:129–139. [PubMed: 6188164]

Wiser AK, Callaway EM. Contributions of individual layer 6 pyramidal neurons to local circuitry in macaque primary visual cortex. J Neurosci. 1996; 16:2724–2739. [PubMed: 8786448]
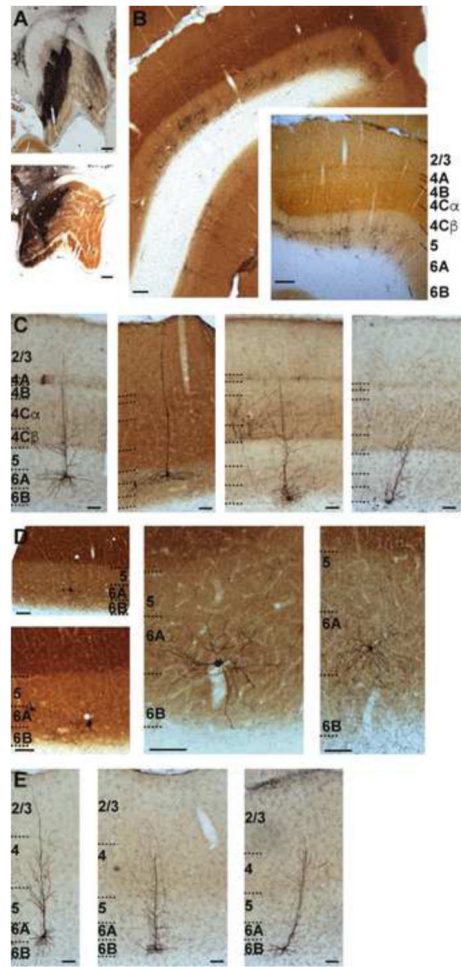
Figure 1.
Injection sites and expression of SAD G-EGFP in CG neurons. **A**. Photographs of injections of virus in LGN in two monkeys indicating approximately the largest extent of each injection (see Supplemental Figure 1A for 3-D renderings of complete injection sites). Scale bars are 500 microns. **B**. Photograph of virus-labeled CG neurons in V1 and V2. Inset is slightly more magnified photograph of labeled CG neurons in V1 to illustrate the sublaminar expression pattern. Scale bars are 200 microns. V1 layers are labeled and indicated by dashed black lines in the inset. Here and throughout, layers 6A and 6B define upper and lower equal halves of layer 6. **C**. Photographs of 4 example V1 CG neurons. Scale bars are 100 microns. Layers are labeled and indicated by black dashed lines. **D**. Higher resolution photographs (showing the deep layers only) of less common morphological types of V1 CG neurons (neurons with large cell bodies [left] and spiny stellate neurons [middle, right]). Scale bars are 50 microns. Layers are labeled and indicated by dashed black lines. **E**. Photographs of 3 example V2 CG neurons. Scale bars are 100 microns. Layers are labeled and indicated by dashed black lines.
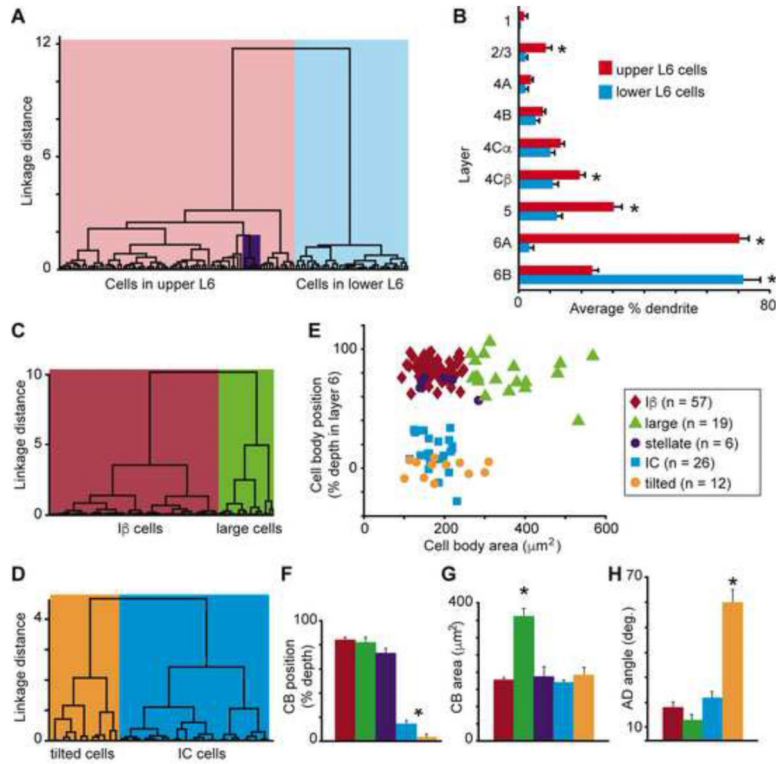
Figure 2.
Classifying V1 CG cell types. **A**. Dendrogram of all V1 CG neurons illustrating the linkage distances, a measurement of clustering, of CG neurons in upper (red) and lower (blue) layer 6 as well as a distinct cluster of spiny stellate neurons within the upper cluster (purple box). **B**. Histogram of average percentage of BD (layer 6) and AD across V1 layers comparing upper (red) to lower (blue) CG neurons. Error bars represent SEMs. Asterisks illustrate significant differences (Bonferroni corrected to p < 0.007). **C**. Dendrogram of clustering of non-stellate upper V1 CG neurons into two classes: IB (dark red) and large (green). **D**. Dendrogram of clustering of lower V1 CG neurons into two classes: IC (blue) and tilted (orange). **E**. Cell body (CB) position as percent depth in layer 6 (0 is white matter border, 1 is layer 5/6 border) versus CB size (square microns) for all V1 CG neurons (labeled according to legend). **F**. Histogram of average CB position as percent depth in layer 6 for V1 CG neurons. Error bars represent SEMs, asterisk indicates that IC and tilted cells are deeper than upper CG neurons (p = 5.1×10^{-7}). **G**. Histogram of average CB size (square microns) for V1 CG neurons. Error bars represent SEMs, asterisk indicates that large cells have larger cell bodies than all other V1 CG neurons (p = 2.2×10^{-9}). **H**. Histogram of average AD angle (degrees relative to vertical) for all V1 CG neurons. Error bars represent SEMs, asterisk indicates that tilted cells have greater AD angles than all other V1 CG neurons (p = 4.6×10^{-8}).
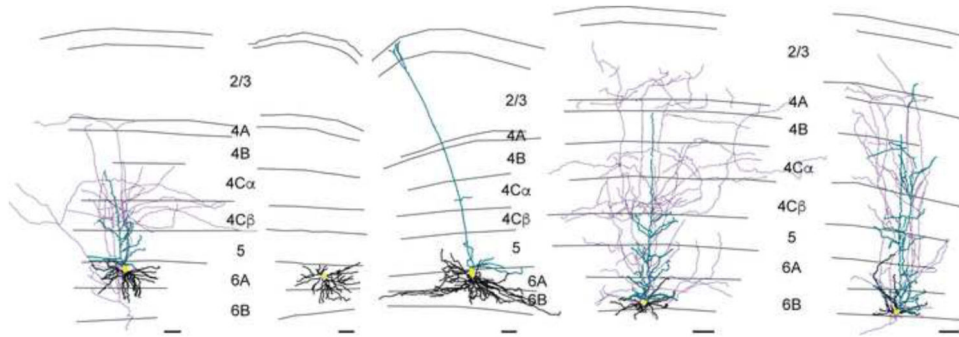
Figure 3.
Example V1 CG neurons of each type. Reconstructions of V1 CG neurons including (left to right) Iβ, spiny stellate, large, IC, and tilted cells. Apical dendrites are illustrated in turquoise, basal dendrites are illustrated in black, axons are illustrated in purple, and cell bodies are illustrated in yellow. Grey lines illustrate laminar borders and layers are labeled for all reconstructions except where layers on neighboring reconstructions are aligned. Scale bars beneath each reconstruction represent 100 microns. For additional reconstructions of each cell type, see Supplemental Figure 3.
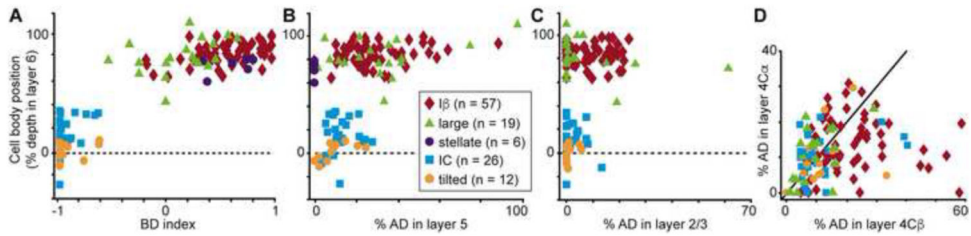
Figure 4.
Dendritic organization of V1 CG neurons. **A**. Cell body (CB) position as percent depth in layer 6 versus index of BD in layer 6A vs. 6B for all V1 CG neurons (labeled according to the legend). Iβ, stellate, large cell indices are significantly different from IC, tilted (Iβ also different from large; p = 4×10-18). **B**. CB position versus percentage of AD in layer 5 for all V1 CG neurons. Iβ, large cells have significantly more AD in layer 5 than the other three cell types (p = 1×10-10). **C**. CB position versus percentage of AD in layer 2/3 for all but stellate V1 CG neurons. Iβ cells have significantly more AD in layer 2/3 than IC and tilted cells (p = 0.007). **D**. Percentage of AD in layer 4Cα versus layer 4Cβ for all but stellate V1 CG neurons. Iβ cells have significantly more AD in 4Cβ than 4Cα (p = 3.9×10-4).
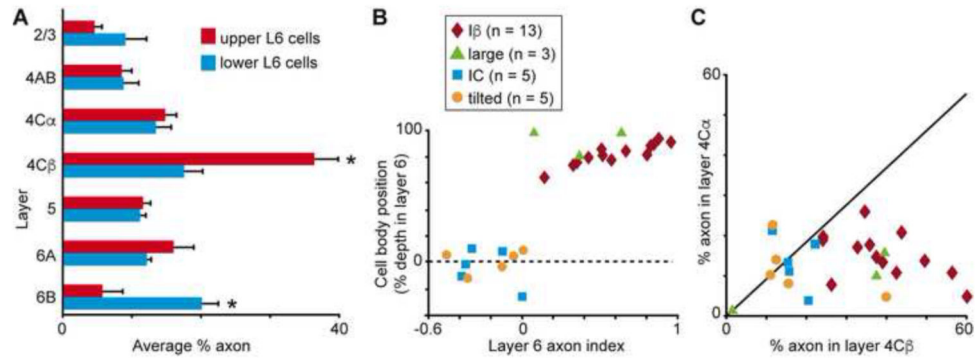
Figure 5.
Local axonal organization for V1 CG neurons. **A**. Histogram of average percentage of axon across the layers in V1 for upper (red) versus lower (blue) V1 CG neurons. Error bars represent SEMs, asterisks indicate significant differences (Bonferroni corrected to p < 0.007). **B**. Cell body (CB) position as percent depth in layer 6 versus index of axon in layer 6A vs. 6B. Indices for Iβ cells are significantly different than those for IC and tilted cells (p = 0.0004). **C**. Percentage of axon in layer 4Cα versus layer 4Cβ. Iβ cells have significantly more axon in 4Cβ than 4Cα (p = 3.3×10-5).
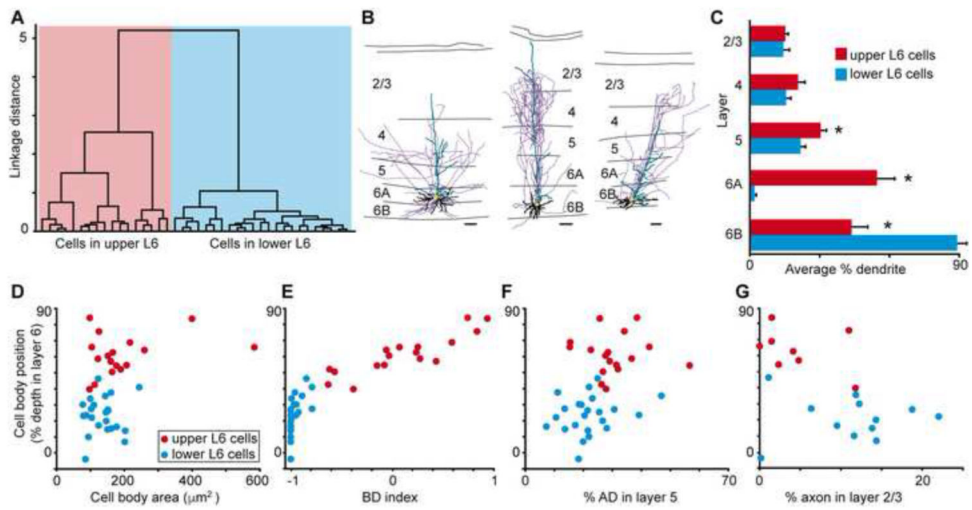
Figure 6.
Classification and analysis of V2 CG neurons. **A**. Dendrogram of all V2 CG neurons illustrating linkage distance, a measure of clustering, of V2 CG neurons positioned in upper (red) and lower (blue) layer 6. **B**. Reconstructions of three V2 CG neurons representing upper (left) and lower (middle, right) groups. Conventions as in Figure 3; scale bars beneath each reconstruction represent 100 microns. **C**. Histogram of average percentage of BD (layer 6) and AD across V2 layers comparing upper (red) to lower (blue) V2 CG neurons. Error bars represent SEMs. Asterisks illustrate significant differences (Bonferroni corrected to $p < 0.003$). **D**. Cell body (CB) position as percent depth in layer 6 versus CB size (square microns) for V2 CG neurons. CB position and size are significantly different for upper and lower V2 CG neurons ($p = 1.5 \times 10^{-7}$ and $p = 0.046$, respectively). **E**. CB position versus indices of BD in layer 6A vs. 6B. Indices for upper and lower V2 CG neurons differ significantly ($p = 6.4 \times 10^{-8}$). **F**. CB position versus percentage of AD in layer 5. Upper V2 CG neurons had significantly more AD in layer 5 compared to lower V2 CG neurons ($p = 0.002$). **G**. CB position versus percentage of axon in layer 2/3. Lower V2 CG neurons had significantly more axon in layer 2/3 than upper V2 CG neurons ($p = 0.03$).
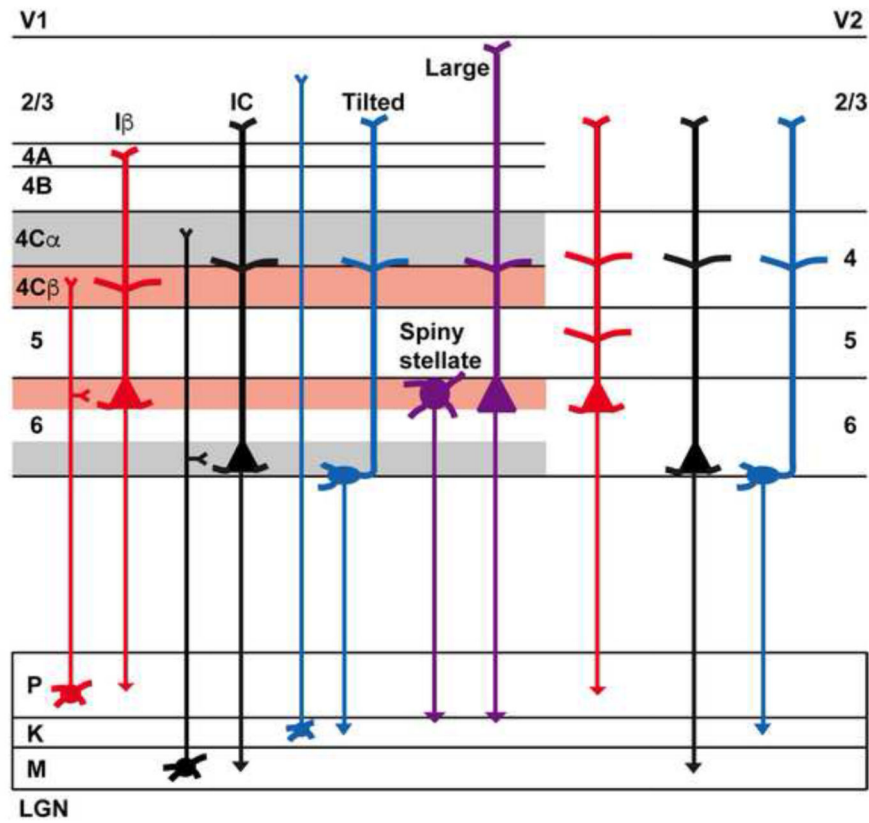
Figure 7.
Schematic representation of CG cell classes in V1 and V2. Red, black, and blue colors represent predicted projections to LGN layers (to parvocellular, magnocellular, and koniocellular LGN layers, respectively) and purple illustrates potential projections of spiny stellate and large CG neurons in V1 to parvocellular and koniocellular layers.